Communication

Binary Superlattices of PbSe and CdSe Nanocrystals

Karin Overgaag, Wiel Evers, Bart de Nijs, Rolf Koole, Johannes Meeldijk, and Daniel Vanmaekelbergh

J. Am. Chem. Soc., **2008**, 130 (25), 7833-7835 • DOI: 10.1021/ja802932m • Publication Date (Web): 31 May 2008

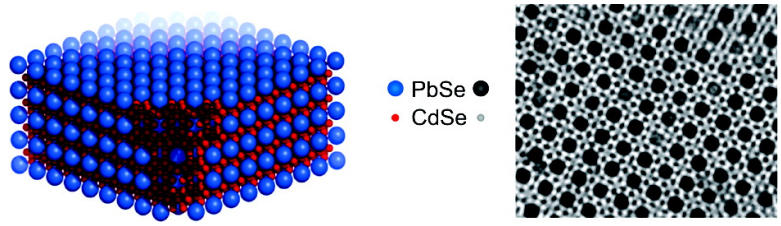

J|A|C|S
COMMUNICATIONS

Published on Web 05/31/2008

Binary Superlattices of PbSe and CdSe Nanocrystals

Karin Overgaag,[†] Wiel Evers,[†] Bart de Nijs,[†] Rolf Koole,[†] Johannes Meeldijk,[‡] and Daniel Vanmaekelbergh*,[†]

Condensed Matter and Interfaces and Electron Microscopy, Debye Institute for NanoMaterials Science, Utrecht University, P.O. Box 80 000, 3508 TA Utrecht, The Netherlands

Received April 21, 2008; E-mail: d.vanmaekelbergh@uu.nl

Studies of the self-organization of micrometer-sized colloids have been extended in the past decade to crystalline building blocks with dimensions in the nanometer range. Superlattices containing one type of colloidal nanocrystals (NCs) (metallic, magnetic, or semiconductor) have been studied in great detail. These studies have been made possible by the availability of NCs with a small dispersion in size and shape and with an excellent control of the surface chemistry. More recently, binary NC superlattices based on metallic,[1] or a combination of metallic and semiconductor building blocks,[2,3] have also been reported; a wide variety in structures and stoichiometry and an astounding long-range order have been demonstrated.[4] Despite the obvious importance for the study of colloidal self-organization and possible applications in novel opto-electronic materials, the combination of two semiconductor-type NCs has been quite limited; binary superlattices combining PbTe and Ag_2Te,[5] and CdSe and CdTe NCs[6,7] have been presented recently.

In the present Communication, we report the formation of binary superlattices consisting of PbSe and CdSe NCs of the AB_2 and cuboctahedral AB_{13} (cub-AB_{13}) type (A = PbSe NC, B = CdSe NC). CdSe and PbSe nanocrystalline quantum dots are the work horses of colloidal nanoscience. The synthesis, electronic structure, quantum confinement, and the optical and electrical properties of both types of NC have been dealt with in numerous studies. Our choice for this particular combination was further motivated by the strong difference in the optical bandgap (PbSe at around 1 eV, CdSe at around 2 eV), which should facilitate the study of collective opto-electronic phenomena. For instance, such a binary superlattice may show a weakly coupled type II band structure,[8,9] featuring long-lived excitons delocalized over PbSe NC/CdSe NC molecular units, thus opening a venue to novel electrical and optical properties beyond that of the individual NCs. In addition, PbSe and CdSe NCs have different crystal structures; this prevents atomic diffusion and alloying upon thermal treatments.[10]

CdSe and PbSe nanocrystals were synthesized by methods described previously in the literature.[11,12] In both cases, the NCs were extracted from the synthesis solution, washed twice, and redispersed in the solvent of interest. In the present work, the CdSe NCs have a trioctylphosphine oxide and hexadecylamine (TOPO and HDA) capping with an effective diameter of 5.8 ± 0.3 nm (core-diameter: 3.4 ± 0.3 nm), while the PbSe NCs have an oleic acid capping (OA) and an effective diameter of 10.3 ± 0.5 nm (core-diameter: 7.3 ± 0.6 nm). The core and effective diameters were obtained from TEM analysis of the single-component NC superlattices, the effective diameter being obtained from the center-to-center distance.

Mixed CdSe NC/PbSe NC suspensions were prepared using toluene, chloroform, and tetrachloroethylene (TCE) as solvents; the NC concentration ratio c_{CdSe}/c_{PbSe} was varied between 1 and 30. The determination of the nanocrystal concentrations is described in the Supporting Information.[13,14] Colloidal crystallization was achieved by evaporation of the solvent from the suspension under reduced pressure at 70 °C, the substrate forming an angle of 30° with the surface of the drying dispersion[3] (Supporting Information, Figure S3). After evaporation, the TEM grids were dipped in ethanol to remove the excess NCs not incorporated into the superlattices and analyzed with a Tecnai 12 and a Tecnai 20 TEM.

The structure and stoichiometry of the deposited NC layers depended strongly on the solvent of the dispersion. Solvent evaporation from toluene and chloroform suspensions resulted in a deposit that consisted of single-component hexagonally ordered PbSe and CdSe NC superlattices and disordered layers, with only a minute percentage (<1%) of binary superlattices. In contrast, mixed dispersions in TCE resulted in deposits with a considerable fraction of binary PbSe−CdSe NC superlattices exhibiting long-range order over micrometers. Below, we only consider the results obtained with TCE. Figures S4 and S5 (Supporting Information) present some large-area overviews of the deposited layers, while Figure 1 presents the observed binary superlattices, AB_2 and AB_{13}, in more detail. Figure 2 presents the results of elemental analysis using STEM-EDX, to show the PbSe and CdSe NC positions in the AB_2 and AB_{13} structures.

The preferential orientation of the AB_2 structure (Figure 1a−c) is with the (0001) plane parallel to the substrate as can be seen by comparison of the TEM image with the same projection of a model AB_2 structure (Figure 1c). AB_2 consists of a simple hexagonal arrangement of large A (PbSe) particles, with the smaller B (CdSe) particles filling all the interstices between the A layers (honeycomb pattern). The elemental analysis along a line scan using STEM-EDX shows clear modulations in the amount of Pb (the maxima indicating the PbSe NCs) in antiphase with the modulation in the Cd amount (indicating the CdSe NCs) in agreement with an AB_2 lattice (Figure 2a). The PbSe center-to-center distance in the (0001) plane is 11.2 nm. The fast Fourier transformation of the TEM image (Figure 1b and Supporting Information S6) is indicative of long-range hexagonal order; the PbSe−PbSe NC center-to-center distance is 10.4 nm, in reasonable agreement with the line scan. Note that the STEM-EDX measurement is prone to thermal drifts. For the AB_{13} structures (Figures 1d−f and g−i), it is clear that the TEM images represent the cuboctahedral AB_{13} (cub-AB_{13}) and not the icosahedral AB_{13}.[15] The preferential crystal orientation is with the (100) plane parallel to the substrate, with a minor fraction of the lattices showing the (110) plane parallel to the substrate (compare with the same projections of the model structures 1f and 1i). The cub-AB_{13} structure consists of a simple cubic lattice of large spheres A (PbSe) with a cuboctahedron cluster of 13 B particles (CdSe) in the body-center of each unit cell. The high degree of order in the AB_{13} structures is obvious from the fast Fourier transforms (Figure

[†] Condensed Matter and Interfaces.
[‡] Electron Microscopy.

10.1021/ja802932m CCC: $40.75

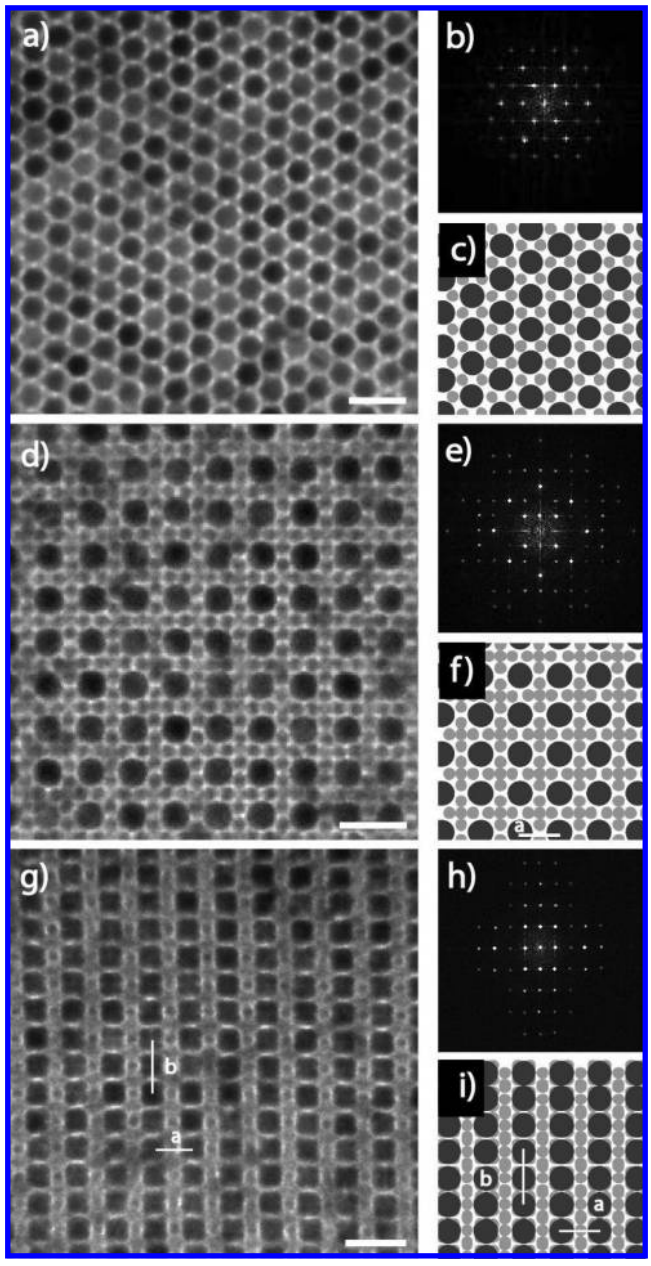

Figure 1. TEM images of binary structures formed with CdSe and PbSe nanocrystals: (a,b,c) an AB_2 structure representing the (0001) plane (a); same projection of a model structure (c); the fast Fourier transform (b). (d,e,f) cub-AB_{13} representing the (100) plane (d); model (f); the fast Fourier transform (e). (g,h,i) cub-AB_{13} with the (110) PbSe terminated (g) ; model (i); the fast Fourier transform (h). All scale bars represent 20 nm.

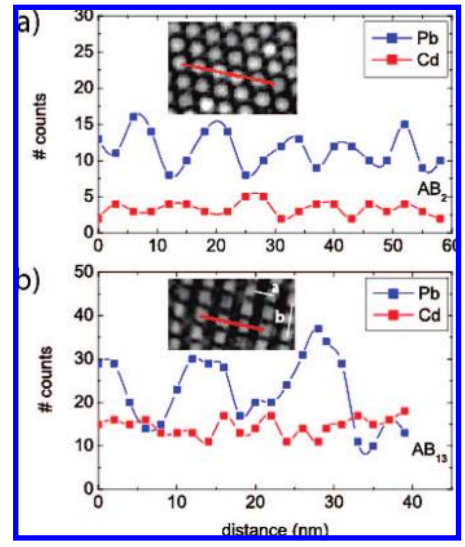

Figure 2. Scanning TEM (STEM) with EDX Cd and Pb element analysis to locate the CdSe and PbSe nanocrystals in binary superlattices. (a): AB_2; line scan in the (0001) plane showing an alternation of maxima in the Pb (blue) and Cd (red) amounts, indicating alternating PbSe and CdSe nanocrystals with a period of 11.2 nm. (b): cuboctahedral AB_{13} (with (110) plane parallel to the substrate), scanned along *a*, showing the positions of the PbSe nanocrystals, the positions of the CdSe nanocrystals are not fully resolved.

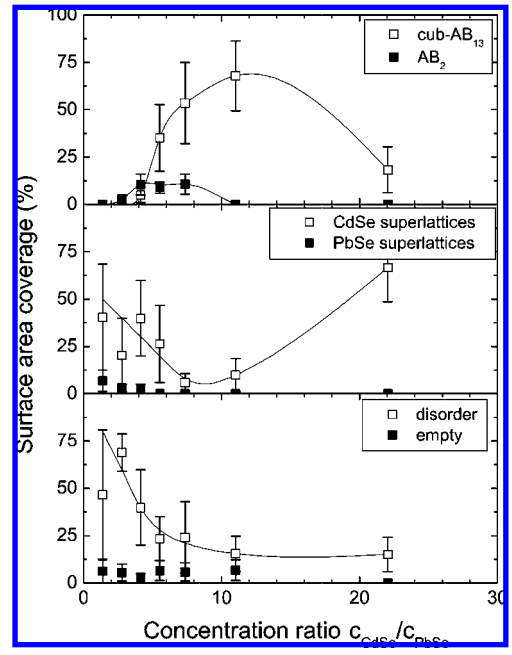

Figure 3. The surface area coverage on the TEM grids with (top panel) AB_2, cub-AB_{13} (A = PbSe, B = CdSe) and (middle panel) single-component CdSe and PbSe superlattices as a function of the concentration ratio of CdSe vs PbSe nanocrystals in the suspensions. The lowest panel shows the relative coverage with disordered layers and the uncovered area. For each concentration ratio, a total area of 4000 μm^2 has been analyzed. The gray solid line represents a guide to the eye.

1e,h). The FFT of the cub-AB_{13} model structures show strong resemblance to the experimental data (see Supporting Information Figure S6). Figure 1d shows the (100) plane with a center-to-center distance between the PbSe NCs of 12.9 nm. Figure 1g shows the (110) plane terminated with additional PbSe NCs from the next parallel plane. This means that the PbSe−PbSe distance indicated in Figure 1g, $b = 17.4$ nm (two times 8.7 nm) and the PbSe−PbSe distance $a = 12.5$ nm, is in good agreement with $17.4/\sqrt{(2)}$ nm and the distance obtained from figure 1d. A STEM-EDX analysis along *a* (Figure 2b) shows clear modulations in the Pb amount, indicating the PbSe NC positions. The resolution was not good enough to resolve the positions of the CdSe NCs.

Now, we discuss the effect of the particle concentration ratio c_{CdSe}/c_{PbSe}, varied between 1 and 30, on the composition and structure of the deposit (Figure 3). At relatively low ratios, that is, $1 < c_{CdSe}/c_{PbSe} < 3$, the deposit consisted mainly of disordered layers (about 65% of the total surface area) and single-component CdSe superlattices (about 30%), with a minor fraction of the PbSe superlattice (about 1%). If c_{CdSe}/c_{PbSe} is increased between 2 and 9, AB_2 superlattices occur on the TEM grids and the surface coverage of AB_2 reaches a maximum of 10% at $c_{CdSe}/c_{PbSe} = 5$

and decreases at larger ratios. The surface coverage by AB_{13} superlattices shows a pronounced peak between $7 < c_{CdSe}/c_{PbSe} < 20$ with a maximum surface coverage of 60% at c_{CdSe}/c_{PbSe} around 12. If the c_{CdSe}/c_{PbSe} ratio is increased above 20, ordered single-component CdSe structures take over at the expense of the AB_{13} superlattices. Figure 3 illustrates that the amounts of binary PbSe $(CdSe)_{13}$ and single-component CdSe NC superlattices are correlated; when the surface coverage of AB_{13} shows a pronounced maximum, that of the single-component superlattice shows a pronounced minimum. To a certain extent, the structure and stoichiometry of the superlattices can be regulated by the relative concentrations of the constituting NCs in the suspension.

The self-organization of micrometer-sized colloids into binary superlattices has been successfully explained on the basis of the hard sphere model.[16,17] In this model, only a steep repulsion at short distance is assumed, which means that the driving force for crystallization is purely entropic. In the limit of high osmotic pressures, the entropic change is positive and maximum if the crystal has the highest packing density.[17]

It is interesting to consider how far the structures that we observe can be explained on the basis of the hard-sphere model. The line of reasoning is similar to that of ref 6 held for superlattices of CdSe and CdTe NCs. The effective diameter of the CdSe and PbSe NCs is 5.8 and 10.3 nm, respectively. For this size ratio of 0.57, the single-component and the AB_2 structure show a filling factor of 0.74, while the filling factor of the cub-AB_{13} is 0.65. On the basis of the hard-sphere model, we must conclude that the single-component and the binary AB_2 structure are the most probable. This is in agreement with our large-scale TEM analysis for $1 < c_{CdSe}/c_{PbSe} < 7$ showing mostly single-component superlattices of CdSe and a maximum of 10% AB_2 structure. However, for $7 < c_{CdSe}/c_{PbSe} < 20$, the cub-$AB_{13}$ superlattice with a filling factor of only 0.65 dominates. This cannot be explained on the basis of the hard-sphere model; interparticle interactions must be important. Van der Waals interactions between the capping molecules increase with the number of nearest neighbors of each PbSe and CdSe nanocrystal. In binary structures, the number of nearest neighbors around the A-site (PbSe) is between 20 (AB_2) and 24 (AB_{13}), hence much larger than for a single-component fcc structure (12), while for the B-site the number is similar to that in a single-component fcc structure (9 for AB_2 or 12 AB_{13}). Therefore, the strong presence of cub-AB_{13} superlattices suggests that van der Waals interactions between adjacent NCs are important for the lattice free energy. The interactions between the capping molecules of adjacent crystals, here OA around PbSe, and TOPO and HDA around CdSe, provide an important contribution to the interparticle van der Waals pair energy. Calculations show that van der Waals forces between two parallel alkane molecules of 10 units can amount to a pair interaction of about 10 kT at room temperature.[6] It is not yet clear if other origins of interparticle interactions should also be taken into account. In this respect, we note that recent cryo-TEM experiments displayed strings of PbSe and CdSe particles in suspension pointing to an electric crystal dipole moment.[18,19] We remark that it is not understood why AB_5 ($CuAu_5$) structures are not observed in the present case. Note that with a combination of CdTe and CdSe NCs, binary AB_5 structures have been reported.[6] The $CuAu_5$ structure has the same filling factor as the cub-AB_{13} at the present size ratio of 0.57, and also a similar number of nearest neighbors. In addition, it is also not clear why in the present case of PbSe and CdSe NCs, crystallization in the solvent TCE leads reproducibly to a large fraction of binary superlattices, while toluene with a two times lower density and similar dielectric constant, and chloroform with a similar density and two times larger dielectric constant, leads to phase segregation. Further experimental and theoretical work is needed for a deeper understanding of nanocrystal self-organization.

The formation of binary superlattices via colloidal crystallization is the most promising method to realize nanostructured architectures in which different materials are positioned in a well-defined 3-D geometry and the NCs are in near contact. In the present case, two types of semiconductor NCs with a strongly different optical gap (PbSe NC around 1 eV, CdSe NC around 2 eV) can be assembled in AB_2 and AB_{13} geometries over large areas. The structures that we obtain are mostly three-dimensional and sufficiently thick for optical applications.

Acknowledgment. Financial support from "NanoNed" (UOE.7012), CW Topgrant 700.53.308, and the European union network "FULLSPECTRUM" (SES6-CT-2003-502620) is gratefully acknowledged. HR TEM experiments were performed by Heiner Friedrich.

Supporting Information Available: Sample preparation and additional TEM images. This material is available free of charge via the Internet at http://pubs.acs.org.

References

(1) Kiely, C. J.; Fink, J.; Brust, M.; Bethell, D.; Schiffrin, D. J. *Nature* **1998**, *396*, 444–446.
(2) Rogach, A. L. *Angew. Chem., Int. Ed.* **2004**, *43*, 148–149.
(3) Redl, F. X.; Cho, K. S.; Murray, C. B.; O'Brien, S. *Nature* **2003**, *423*, 968–971.
(4) Shevchenko, E. V.; Talapin, D. V.; Kotov, N. A.; O'Brien, S.; Murray, C. B. *Nature* **2006**, *439*, 55–59.
(5) Urban, J. J.; Talapin, D. V.; Shevchenko, E. V.; Kagan, C. R.; Murray, C B. *Nat. Mater.* **2007**, *6*, 115–121.
(6) Chen, Z. Y.; Moore, J.; Radtke, G.; Sirringhaus, H.; O'Brien, S. *J. Am. Chem. Soc.* **2007**, *129*, 15702–15709.
(7) Chen, Z.; O'Brien, S. *ACS Nano*, published online May 7, 2008, http://dx.doi.org/10.1021/nn800129s.
(8) Kim, S.; Fisher, B.; Eisler, H. J.; Bawendi, M. *J. Am. Chem. Soc.* **2003**, *125*, 11466–11467.
(9) Chin, P. T. K.; de Mello Donegà, C.; van Bave, S. S.; Meskers, S. C. J.; Sommerdijk, N. A. J. M.; Janssen, R. A. J. *J. Am. Chem. Soc.* **2007**, *129*, 14880–14886.
(10) Kudera, S.; Carbone, L.; Casula, M. F.; Cingolani, R.; Falqui, A.; Snoeck, E.; Parak, W. J.; Manna, L. *Nano Lett.* **2005**, *5*, 445–449.
(11) de Mello Donegà, C.; Hickey, S. G.; Wuister, S. F.; Vanmaekelbergh, D.; Meijerink, A. *Phys. Chem. B* **2003**, *107*, 489–496.
(12) Houtepen, A. J.; Koole, R.; Vanmaekelbergh, D. L.; Meeldijk, J.; Hickey, S. G. *J. Am. Chem. Soc.* **2006**, *128*, 6792–6793.
(13) Moreels, I.; Lambert, K.; De Muynck, D.; Vanhaecke, F.; Poelman, D.; Martins, J. C.; Allan, G.; Hens, Z. *Chem. Mater.* **2007**, *19*, 6101–6106.
(14) Yu, W. W.; Qu, L.; Guo, W.; Peng, X. *Chem. Mater.* **2003**, *15*, 2854–2860.
(15) Shevchenko, E. V.; Talapin, D. V.; O'Brien, S.; Murray, C. B. *J. Am. Chem. Soc.* **2005**, *127*, 8741–8747.
(16) Murray, M. J.; Sanders, J. V. *Phil. Mag. A* **1980**, *42*, 721.
(17) Eldridge, M. D.; Madden, P. A.; Frenkel, D. *Nature* **1993**, *365*, 35–37.
(18) Klokkenburg, M.; Houtepen, A. J.; Koole, R.; de Folter, J. W. J.; Erné, B. H.; van Faassen, E.; Vanmaekelbergh, D. *Nano Lett.* **2007**, *7*, 2931–2936.
(19) Talapin, D. V.; Shevchenko, E. V.; Murray, C. B.; Titov, A. V.; Král., P. *Nano Lett.* **2007**, *7*, 1213–1219.

JA802932M